Science Translational Medicine
AAAS

Supplementary Materials for

Prevalence of intratumoral regulatory T cells expressing neuropilin-1 is associated with poorer outcomes in patients with cancer

Christopher A. Chuckran *et al.*

Corresponding author: Dario A. A. Vignali, dvignali@pitt.edu; Tullia C. Bruno, tbruno@pitt.edu

Sci. Transl. Med. **13**, eabf8495 (2021)
DOI: 10.1126/scitranslmed.abf8495

The PDF file includes:

Figs. S1 to S13
Tables S1 and S2

Other Supplementary Material for this manuscript includes the following:

Data file S1

Supplementary Materials:

A

Indication	Tissue	Total n	Gender Ratio (%M:%F)	Age (Mean ± SD)
HNSCC	Blood	85	73:27	60 (±12)
	Tumor	61		
OvCa	Blood	12	0:100	62 (±13)
	Tumor	49		
NSCLC	Blood	37	43:57	71 (±9.3)
	Tumor	13		
CRC	Blood	15	38:62	63 (±12.9)
	Tumor	12		
PDAC	Blood	13	27:73	70 (±8.9)
	Tumor	12		
Melanoma	Blood	34	55:45	54 (±15.8)
	Tumor	32		
TOTAL		*375*		

B

	Tissue	Total n	Gender Ratio (%M:%F)	Age (Mean ± SD)
HD	Blood	30	43:57	43 (±16)
	Tonsil	9	67:33	33 (±10)
	Lung (Normal)	9	36:64	59 (±15)
	Lung (COPD)	6	33:67	63 (±4.5)
	Ovary	14	0:100	50 (±17)
	Blood (ovarian cyst patients)	17	0:100	57 (±17)
TOTAL		*85*		

C

	Above HD PBL Max. % $NRP1^{SURF+}$	
	PBL	TIL
HNSCC	15 / 85 (17.6%)	30 / 61 (49.2%)
OvCa	2 / 12 (16.7%)	32 / 49 (65.3%)
NSCLC	8 / 37 (21.6%)	5 / 13 (38.5%)
CRC	4 / 15 (26.7%)	5 / 12 (41.7%)
PDAC	6 / 13 (46.2%)	5 / 12 (41.7%)
TOTAL	*35 / 162 21.6%*	*77 / 147 52.4%*

D

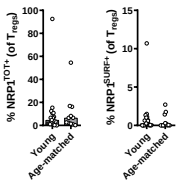

		Total n	Gender Ratio (%M:%F)	Age (Mean ± SD)
HD PBL	Young	17	41:59	33 (±10.1)
	Age-Matched	13	46:54	59 (±7.4)
TOTAL		*30*		

Fig. S1. Demographics of patients with cancer and healthy donor cohorts are comparable and indicate neuropilin-1 expression is associated with cancer rather than age. (A) A summary of patient samples used in this study with gender and age distributions for the cohorts reported is shown. HNSCC, head & neck squamous cell carcinoma; OvCa, ovarian cancer; NSCLC, non-small cell lung cancer; CRC, colorectal cancer; PDAC, pancreatic ductal adenocarcinoma. **(B)** A brief summary of healthy donor (HD) samples used in this study is shown with gender and age distributions for the cohorts reported for comparison to the cohorts of patients with cancer. COPD, chronic obstructive pulmonary disease. **(C)** The proportion of patient samples which had a higher prevalence of $NRP1^{SURF+}$ regulatory T (T_{reg}) cells than any HD PBL sample measured is tabulated. The maximum % $NRP1^{SURF+}$ sample from a HD was 10.7%; however, it should be noted that

this is a conservative representation of the difference between patients with cancer and HDs as the second highest HD PBL measurement was 2.70%. **(D)** The healthy donor peripheral blood (PBL) cohort is shown divided into a “young” fraction (n=17) or an “age-matched” fraction (n=13) whose age distribution largely overlapped with our cohorts of patients with cancer (defined as greater than 50 years of age). We found no difference in neuropilin-1 (NRP1) expression between these groups of healthy individuals. Bars represent the median of the distribution.

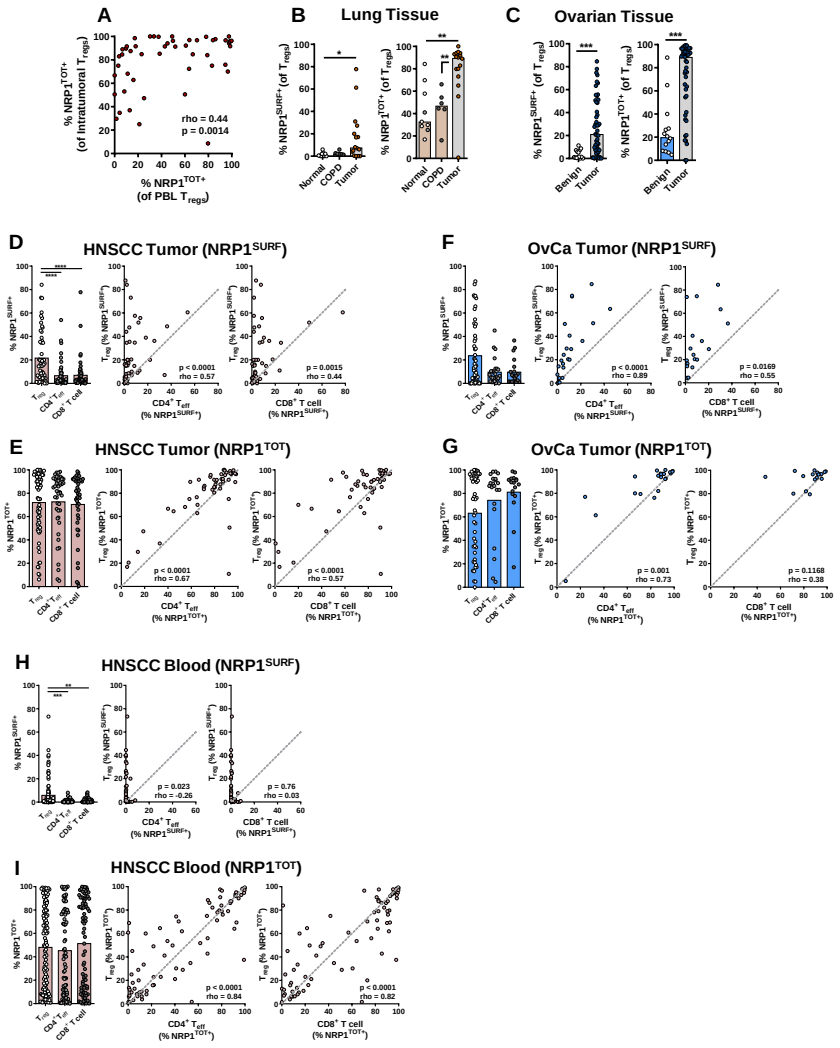

Fig. S2. Non-cancer tissues have few NRP1$^+$ T$_{regs}$ and NRP1 expression is distinct between T cell subsets. (A) Expression of NRP1^{TOT} on T$_{regs}$ from patients with HNSCC is matched between tumor biopsy and peripheral blood (n=50). Spearman's non-parametric correlation analysis results reported. **(B)** Expression of NRP1 by T$_{regs}$ in non-cancer lung tissue specimens (n=9 for normal and n=6 for COPD) versus non-small cell lung cancer (n=16) is shown. Non-cancer participants who smoke are indicated as gray dots. Bar indicates median. Data were analyzed using a non-parametric Kruskal-Wallis test with 5% FDR. *q<0.05; **q<0.01. **(C)** Expression of NRP1 by T$_{reg}$ cells in non-cancer ovary

tissue specimens (n=14) is compared to those from ovarian cancer (n=47). Bar indicates median. Data were analyzed using a non-parametric Kolmogorov-Smirnov test. ***p<0.001. **(D)** The percentage of each indicated T cell subset (T_{reg} cells, $CD4^+$ T_{eff} cells, and $CD8^+$ T cells) that expresses $NRP1^{SURF}$ and the correlation of $NRP1^{SURF}$ expression between T_{reg} cells and the indicated subsets is shown for HNSCC tumors (n=50). Bar indicates mean. Data were analyzed using a non-parametric Kruskal-Wallis test with 5% FDR. *q<0.05; **q<0.01; ***q<0.001; ****q<0.0001. Spearman's non-parametric correlation analysis results are reported for plots on right. **(E)** Same as D but for OvCa (n=23). **(F)** Same as D but for $NRP1^{TOT}$ (n=50). **(G)** Same as F but for OvCa (n=23). **(H and I)** Same as D and F but for HNSCC PBL samples (n=79).

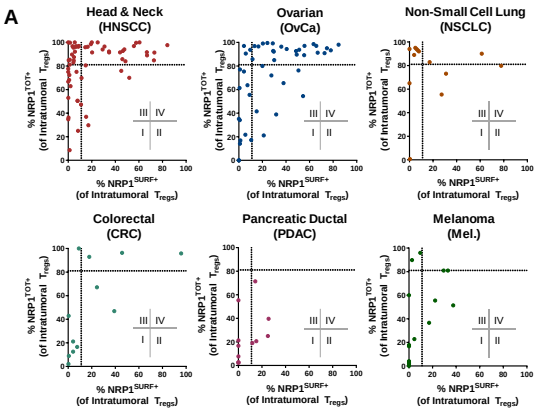

B

	n	NRP1 Expression Surface (median)	NRP1 Expression Total (median)	Correlation P-value	Correlation rho	Distribution of patients I	II	III	IV
HNSCC	61	8.89%	89.0%	0.0061	0.35	24.6%	9.8%	27.9%	37.7%
OvCa	47	24.2%	89.2%	0.0001	0.56	27.7%	17.0%	6.4%	48.9%
NSCLC	13	7.0%	89.0%	0.5940	-0.16	15.4%	23.1%	46.2%	15.4%
CRC	12	8.4%	44.9%	0.0041	0.78	50.0%	16.7%	8.3%	25.0%
PDAC	12	0%	19.8%	0.0546	0.58	58.3%	41.7%	0%	0%
Mel.	15	2.6%	36.6%	0.0102	0.65	53.3%	33.3%	13.3%	0%

C

Tumor Samples Only

Pathological Stage	
0 or 1	0
2	4
3	8
4	3
Not reported	3
Data not available	14

D

All Samples

Prior therapy	
None	11
Immunotherapy (IL-2, HD IFN, or ICB)	7
Plaque radiation	2
Treme. + Dabra.	1
Multiple	4
Not reported	19

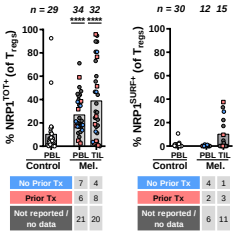

Fig. S3. NRP1 expression distribution differs across solid tumors. (A) Distribution of intratumoral T_{reg} NRP1 expression for all solid tumor types are reported. Differences may be due to differential tissue microenvironment or states of anti-tumor inflammation. Quadrants are defined by the median $NRP1^{SURF}$ and $NRP1^{TOT}$ expression for the aggregate data set (all tumors combined $NRP1^{SURF}$ 11.10%; $NRP1^{TOT}$ 82.95%). **(B)** The table summarizes measures of NRP1 distributions from (A), depicts correlation between $NRP1^{SURF}$ and $NRP1^{TOT}$ for each tumor, and the percentage of samples from that tumor of origin which fall into each quadrant. Spearman's non-parametric correlation analysis results are reported in columns 4 and 5. **(C)** The pathology-defined stage of melanoma tumor samples collected is shown. Most samples were stage 3 or 4, which is metastatic disease. There were not enough samples to determine if there is a meaningful difference in NRP1 expression between patients with stage 2 and stage ¾ disease. Though clinical data were not available for a fraction of patients with melanoma analyzed in this study,

our analysis did not change if those participants were excluded. **(D)** Treatment (Tx) history prior to sample collection for all patients with melanoma whose samples were analyzed are shown on the left with color-coded expression profiles (similar to Figure 1B and C) shown on the right. The melanoma cohort was the only cohort which analyzed pre-treated samples. Differences in NRP1 expression based on pre-treatment were not apparent. Additionally, those individuals without treatment history available were evenly distributed within the same range as those for which it was recorded. Bar indicates mean. A non-parametric Kruskal-Wallis test was used with 5% FDR. ****$q<0.0001$.

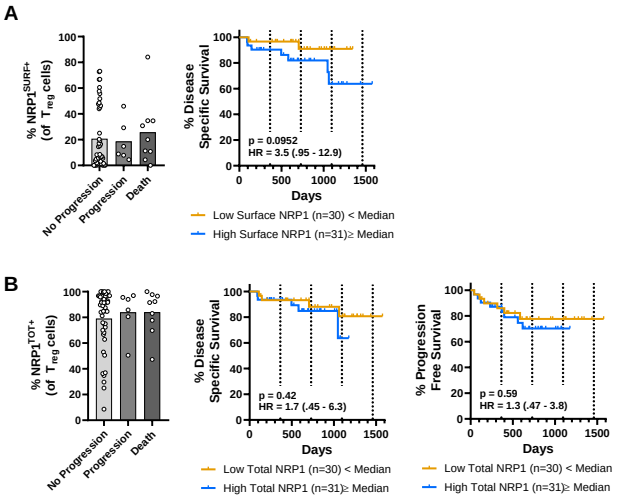

Fig. S4. Analysis of NRP1 as a predictor of clinical outcome in HNSCC. (A) $NRP1^{SURF}$ expression between patients that never progressed (n=46), progressed but are alive (n=6), or those who died due to their disease (n=9). Bar indicates mean. Disease specific survival (DSS) curve comparison was executed using the logrank Mantel-Cox test. P-value with the hazard ratio (HR) with a 95% confidence interval is reported. Data matches cohort from Figure 1G. **(B)** $NRP1^{TOT}$ expression between patients that never progressed (n=46), progressed but are alive (n=6), or those who died due to their disease (n=9). Bar indicates mean. Progression-free survival and DSS curve comparisons were executed using the logrank Mantel-Cox test. P-value with the hazard ratio (HR) with a 95% confidence interval is reported. Data matches cohort from Figure 1G.

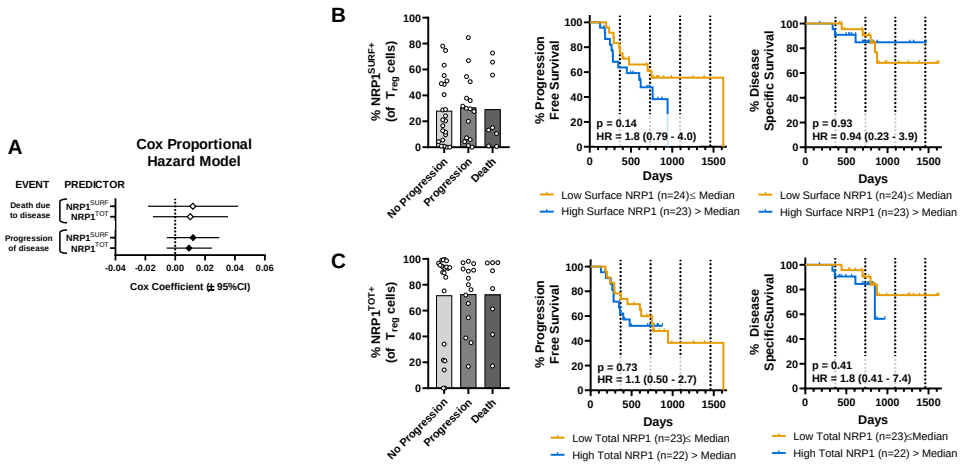

Fig. S5. Analysis of NRP1 as predictor of clinical outcome in OvCa. (A) Univariate Cox proportional hazard model for $NRP1^{SURF}$ and $NRP1^{TOT}$ as continuous predictors of PFS and DSS. Cox coefficient reported ± the 95% confidence interval. **(B)** $NRP1^{SURF}$ expression between patients that never progressed (n=23), progressed but are alive (n=16), or those who died due to their disease (n=8). Bar indicates mean. DSS curve comparison was executed using the logrank Mantel-Cox test. P-value with the hazard ratio (HR) with a 95% confidence interval is reported. Data matches cohort from Figure 1G. **(C)** $NRP1^{TOT}$ expression between patients that never progressed (n=23), progressed but are alive (n=16), or those who died due to their disease (n=8). Bar indicates mean. Progression-free survival and DSS curve comparisons were executed using the logrank Mantel-Cox test. P-value with the hazard ratio (HR) with a 95% confidence interval is reported. Data matches cohort from Figure 1G.

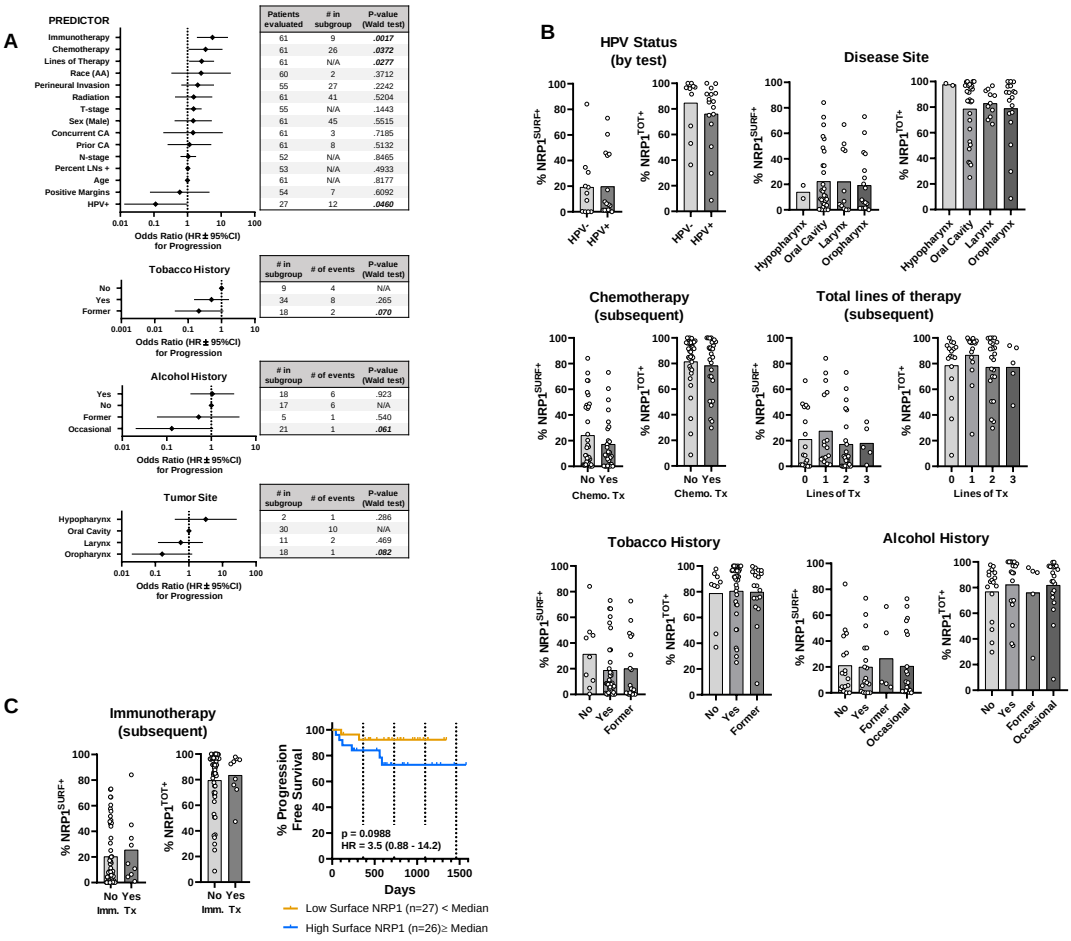

Fig. S6. Analysis of clinical parameters and covariates in HNSCC cohort does not reveal any confounding factors. (A) All other relevant clinical characteristics were tested for their contribution to disease progression using iterative, univariate Cox proportional hazard models. For the first group, the number of participants evaluated for that characteristic, the number of participants who are in the category (9 of 61 participants did receive immunotherapy), and the corresponding p-value, calculated by the Wald test, are reported. P-values are bold and italic if they were below 0.10 in the Wald test. For the three lower groups, the number of individuals within each subgroup and the number of recurrence events within that group are reported. **(B)** For those parameters which had p-values below 0.10 for the Wald test, the distribution of $NRP1^{SURF}$ and $NRP1^{TOT}$

expression is plotted. NRP1 expression was not significantly different across any of these parameters by the Kruskal-Wallis test was used with 5% FDR or non-parametric Kolmogorov-Smirnov test as appropriate. Number of patients in each subgroup is reported in (A). **(C)** NRP1 expression divided by subsequent immunotherapy treatment. Removing these participants from our survival analysis from Figure 1G produced the Kaplan-Meyer curve on the right. Bar indicates mean. Differences in distribution were tested using the non-parametric Kolmogorov-Smirnov test. Curve comparison was executed using the logrank Mantel-Cox test.

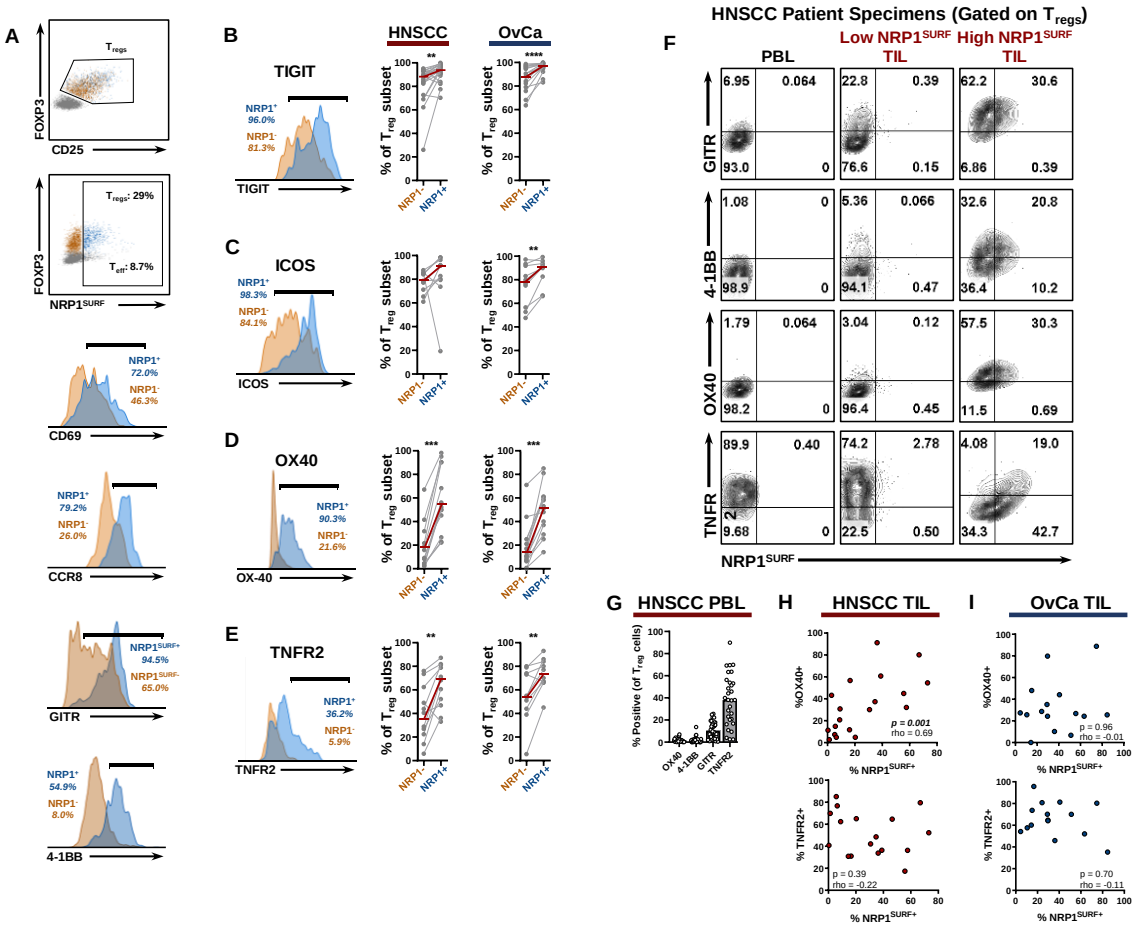

Fig. S7. Intratumoral NRP1 expression is associated with an increased activation phenotype. (A) Representative gating for analysis in Fig. 2 and the remainder of fig. S6 is shown. The sample shown is from a HNSCC tumor. NRP1^{SURF+} indicated as NRP1^{+} for remainder of the figure. **(B to E)** Representative plots (HNSCC) and graphs for expression of indicated markers are shown. HNSCC graphs are on left and OvCa graphs are on the right. Number of samples ranges from 10 to 22 depending on marker and tumor type. Expression of the indicated markers was compared between NRP1^{+} and NRP1^{-} intratumoral T_{regs} using a paired, non-parametric t-test (Wilcoxon). **p<0.01; ***p<0.001; ****p<0.0001. **(F)** Representative staining for co-expression of NRP1^{SURF} and tumor necrosis factor super family (TNFRSF) members used in this analysis is

shown. Fresh tumor and blood samples were stained immediately after processing. **(G)** Tabulation of peripheral blood expression of TNFRSFs in patients with HNSCC is shown. Bars represent the mean with sample numbers ranging from 29 to 42 depending on marker. **(H)** Correlation plots are shown for OX40 (n=19) and TNFR2 (n=17) with $NRP1^{SURF}$ in HNSCC. Spearman's correlation coefficients and non-parametric p-values are reported. **(I)** Correlation plots are shown for OX40 (n=15) and TNFR2 (n=15) with $NRP1^{SURF}$ in OvCa. Spearman's correlation coefficients and non-parametric p-values are reported.

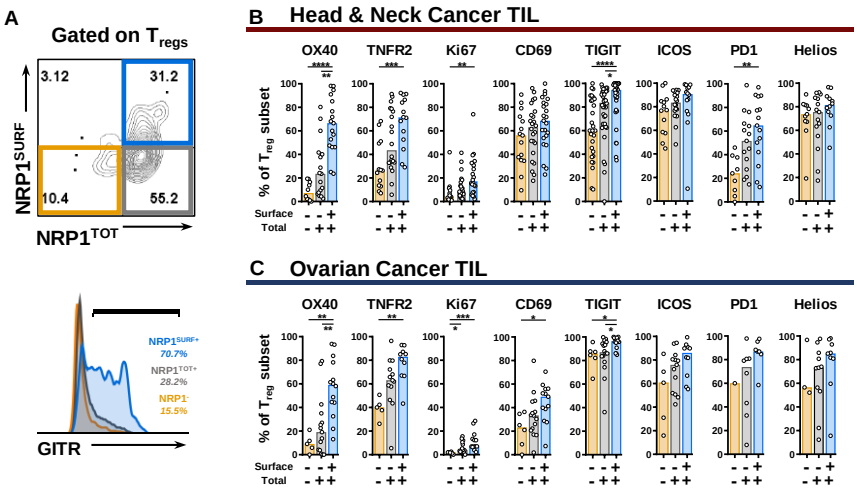

Fig. S8. Intratumoral NRP1^{TOT} expression is associated with an intermediate phenotype between NRP1^{-} and NRP1^{SURF+} T$_{reg}$ cells. (A) Representative gating from an HNSCC tumor used for analysis in B and C is shown. **(B and C)** Analysis of markers shown in Fig. 2 and fig. S7 but reanalyzed to discriminate between T$_{reg}$ cells that are completely NRP1 negative versus those that express the protein but do not have it on the cell surface (Total+, Surface-) or that express protein and have it on the cell surface (Total+, Surface+) is shown. Bars indicate the median. Samples per subgroup range from 1 to 38 depending on marker and T$_{reg}$ subgroup. Differences between the three sub-populations were assessed by non-parametric Kruskal-Wallis test with a 5% FDR. *q<0.05; **q<0.01; ***q<0.001; ****q<0.0001.

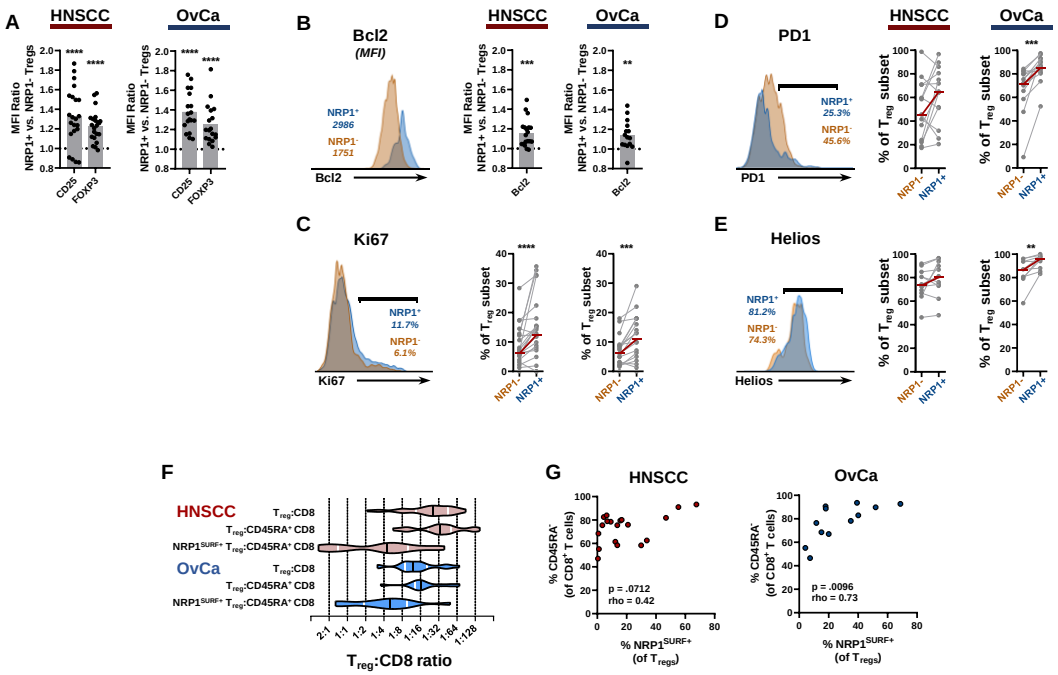

Fig. S9. Intratumoral NRP1^{SURF+} T_{reg} are more stable and correlate with CD45RA^{-} CD8^{+} T cell infiltration. (A) Mean fluorescence intensity (MFI) of FOXP3 and CD25 were measured on intratumoral T_{regs} by flow cytometry (n=22 HNSCC, n=18 OvCa). Data is shown as a ratio to the MFI of matched NRP1^{-} T_{regs} where the bar indicates the mean. A one sample two-tailed t-test was used to evaluate if the ratio was equal to 1.0. ****p<0.0001. **(B and C)** Intratumoral NRP1^{SURF+} T_{regs} (referred to as NRP1^{+} for remainder of figure) have increased markers of survival and proliferation as indicated by B-cell lymphoma 2 (Bcl2) and Ki67 expression. Bcl2 is reported by similar means as FOXP3 and CD25 and assessed by one-sample two-tailed student's t-test with **p<0.01; ***p<0.001 (n=19 HNSCC, n=15 OvCa). Ki67 is reported as the percentage of the T_{reg} sub-population (either NRP1^{+} or NRP1^{-}) expressing the marker (n=22 HNSCC, n=18 OvCa). Expression between NRP1^{+} and NRP1^{-} T_{regs} was compared using a paired, non-parametric t-test (Wilcoxon). The median values for each subset are shown as red bars

over the individual data points. ***p<0.001; ****p<0.0001. **(D and E)** Representative plots (HNSCC) and graphs for expression of indicated markers are shown. HNSCC graph is on left and OvCa is on the right (number of samples range from 10 to 14 depending on marker and tumor type). Expression of the indicated markers was compared between $NRP1^{+}$ and $NRP1^{-}$ intratumoral T_{regs} was compared using a paired, non-parametric t-test (Wilcoxon). **p<0.01; ***p<0.001; ****p<0.0001. **(F)** The ratio of intratumoral T_{regs} to $CD8^{+}$ T cells in both HNSCC and OvCa were tabulated (n=19 HNSCC, n=12 OvCa). The length of the violin plot represents the data range, and the bar thickness reflects the abundance of samples. For each tumor, three ratios were calculated and reported: the ratio of all T_{regs} to all $CD8^{+}$ T cells, the ratio of all T_{regs} to $CD45RA^{-}$ $CD8^{+}$ T cells, and the ratio of $NRP1^{SURF+}$ T_{regs} to $CD45RA^{-}$ $CD8^{+}$ T cells. The black line indicates the median and the white lines indicate the quartiles. **(G)** The prevalence of $NRP1^{SURF+}$ T_{regs} and $CD45RA^{-}$ $CD8^{+}$ T cells (within their respective T cell compartments) are plotted (n=19 HNSCC, n=12 OvCa). Nonparametric (Spearman's) correlation output is reported.

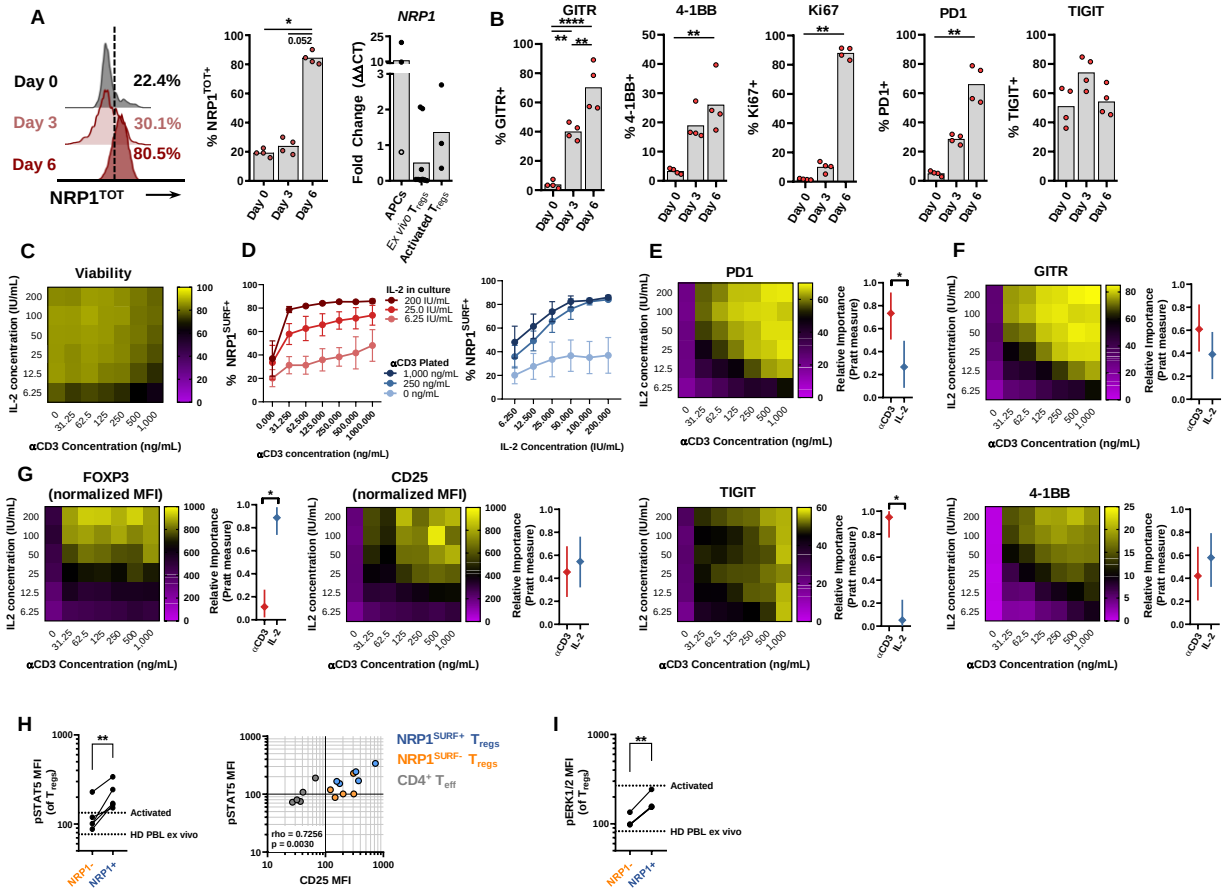

Fig. S10. NRP1 co-expression module. (A) $NRP1^{TOT}$ expression kinetics with in vitro stimulation (n=4) and reverse transcription quantitative polymerase chain reaction (RT-qPCR) for NRP1 gene transcription comparing resting (ex vivo, n=9) T_{reg} cells and in vitro activated T_{reg} cells (n=3). Bars represent the mean. Differences between the three timepoints were assessed by non-parametric Kruskal-Wallis test with a 5% FDR. *q<0.05. **(B)** Upregulation of additional activation markers during same experiment are shown as in (A). Bars represent the mean. Differences between the three sub-populations were assessed by non-parametric Kruskal-Wallis test with a 5% FDR. **q<0.01; ****q<0.0001. **(C)** Cell viability at end of assay is shown for samples from Fig. 3B across conditions from four independent experiments. **(D)** Individual curves for the

indicated conditions are shown as the mean ± standard deviation of four independent experiments. Left (red) shows the CD3-dependent effect for $NRP1^{SURF}$ expression and right (blue) shows the interleukin (IL)-2-dependent effect for $NRP1^{SURF}$ expression. **(E to G)** Heatmaps with Pratt measure plots are shown for indicated markers to compare with NRP1 in Fig. 3B of four independent experiments. The diamond represents the computed Pratt measure with the arms representing the 95% confidence interval. *p<0.05. **(H)** Ex vivo intratumoral T_{regs} (n=5) were stained for phosphorylated signal transducer and activator of transcription 5 (pSTAT5) after a 15-minute in vitro IL-2 treatment. The dashed lines indicate the expression level for the biological positive and negative controls (activated T cells and ex vivo lymphocytes respectively). Data were analyzed using a paired, non-parametric t-test (Wilcoxon). **p<0.01. T_{eff}, effector T cell. **(I)** Phosphorylated extracellular signal-regulated kinase 1/2 (pERK1/2) is shown for the same samples (n=5; some samples overlapping and not visible). The dashed lines indicate the expression level for the biological positive and negative controls (activated T cells and ex vivo lymphocytes respectively). Data were analyzed using a paired, non-parametric t-test (Wilcoxon). **p<0.01.

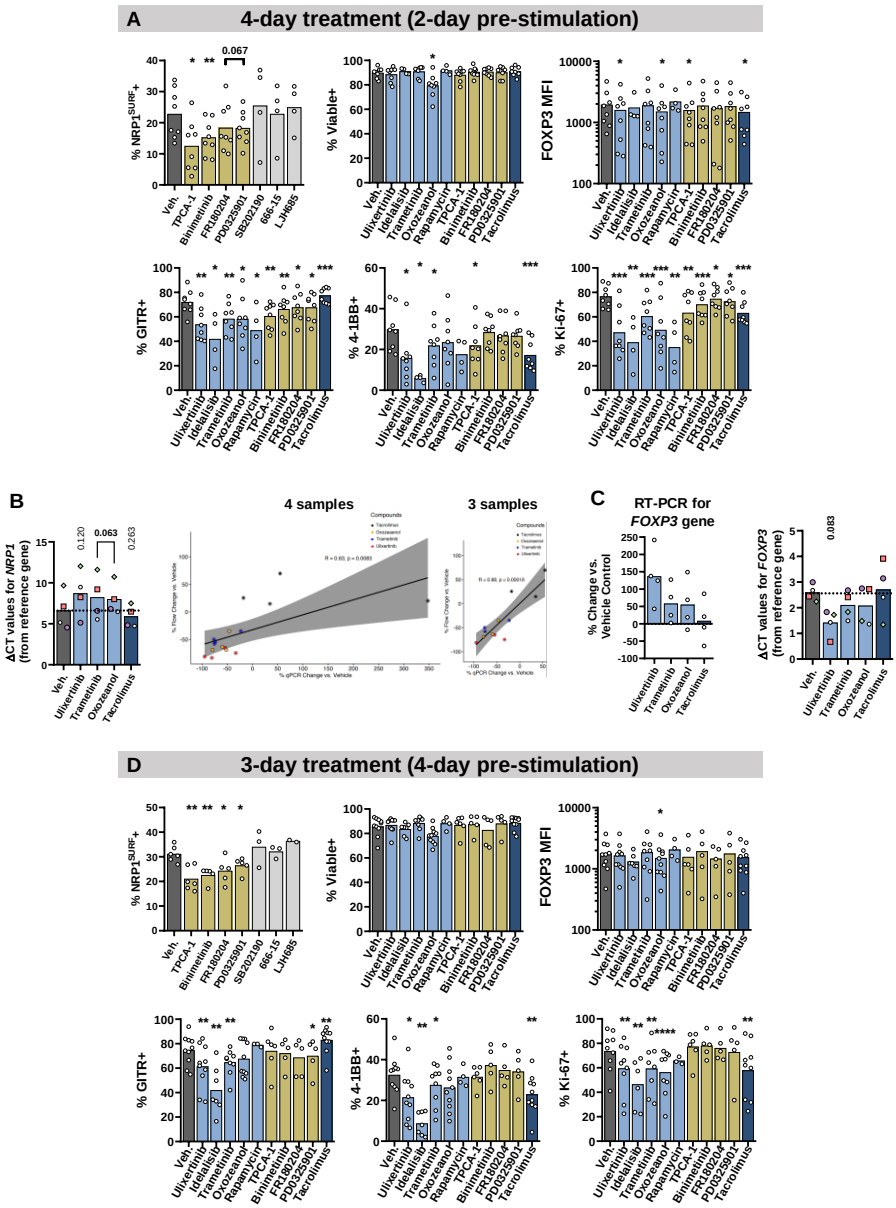

Fig. S11. MAPK pathway among top regulators of NRP1^{SURF}. (A) Additional kinases that attenuated NRP1^{SURF} upregulation are shown in the first graph. Results are tabulated from four to ten independent experiments, depending on the inhibitor. Subsequent panels show the impact of these agents (in yellow) and those from the Fig. 3 (blue) for the indicated proteins or markers. Agents corresponding to gray bars did not have an effect on NRP1^{SURF} upregulation. There were no major differences in cell viability observed

due to treatment, with the exception of oxozeaenol. Bars represent the mean. Because some conditions only had fewer replicates, distributions were evaluated using a mixed effects model and each condition was compared to the vehicle control. *q<0.05; **q<0.01; ***q<0.001; ****q<0.0001. **(B)** Same as in (A) but for the four-day pre-stimulation experiment. **(C)** Delta CT (ΔCT) values are shown for the *NRP1* gene following four-day inhibitor treatment (with four-day pre-stimulation). Data were analyzed using a repeated measures one-way ANOVA versus the vehicle only condition with a 5% FDR adjustment. Each point is color coded by donor. On the right, the percent change in *NRP1* transcript by RT-qPCR is correlated to the percent change in $NRP1^{SURF}$ protein by flow cytometry. R and p-value are reported for correlation. The points are color coded by inhibitor treatment. The first graph includes all 4 donors; however, a possible outlier in the tacrolimus-treated group may have skewed the best fit analysis. Thus, we excluded all conditions from the affected donor, and presented the graph with 3 donors to the right for comparison. **(D)** *FOXP3* gene transcription by RT-qPCR is reported for the same samples and conditions in (C). The first plot shows the percent change versus the vehicle control, and the right plot shows the raw ΔCT values. Data were analyzed using a repeated measures one-way ANOVA versus the vehicle only condition with a 5% FDR adjustment. Each point is color coded by donor.

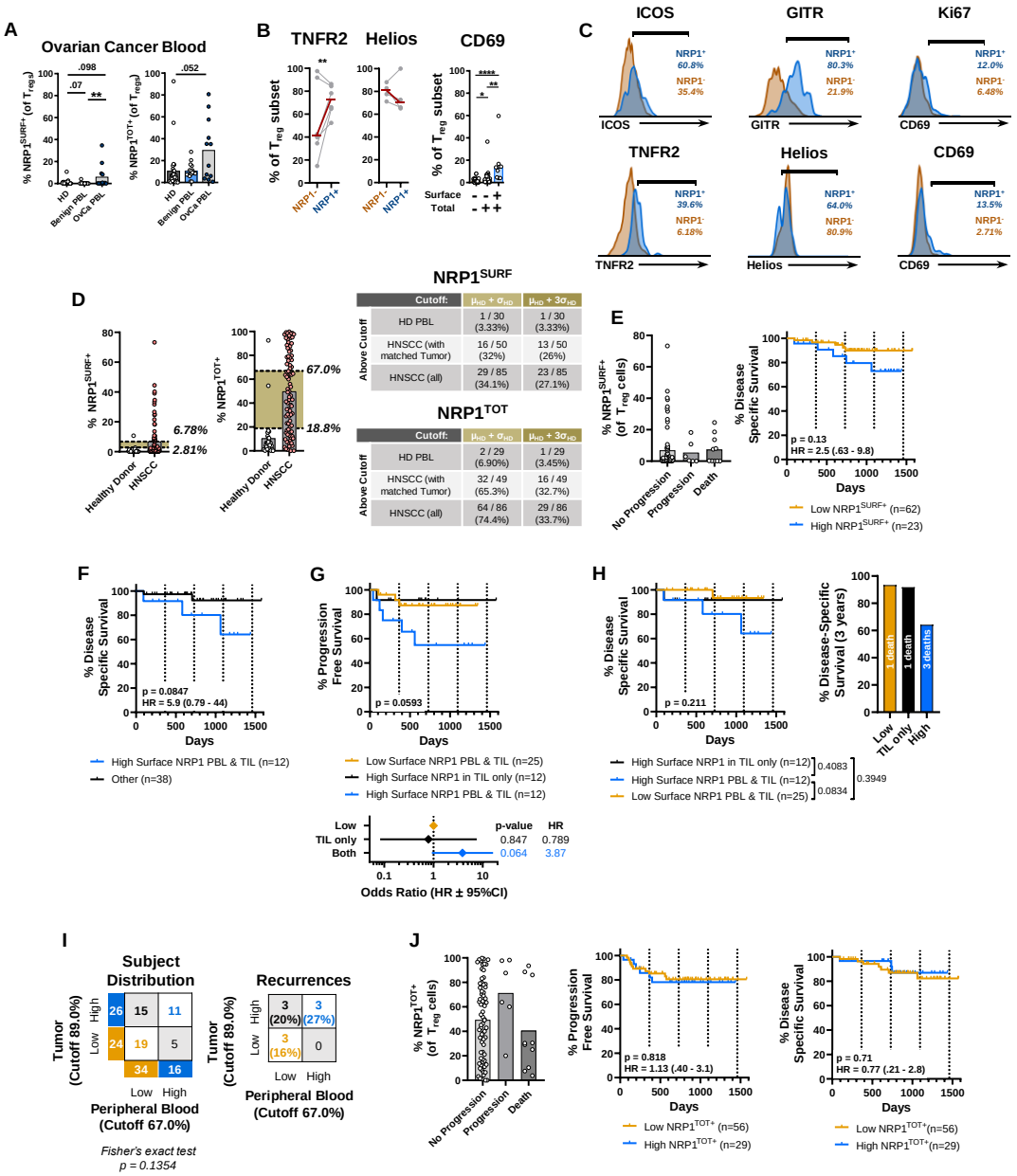

Fig. S12. Analysis of peripheral blood T_{reg} NRP1 expression as an indicator of clinical outcome in HNSCC. (A) Peripheral blood T_{reg} expression of both $NRP1^{SURF}$ and $NRP1^{TOT}$ is shown for patients who had an ovarian lesion removed (n=16) and compared to that of healthy donors (n=29) or those with malignant tumors (n=12). Assignment of benign versus malignant was determined by a pathologist. Data were analyzed using a non-parametric Kruskal-Wallis test with FDR of 5%. **p<0.01. **(B)** Paired expression for

TNFR2 (n=6) and Helios (n=4) similar to Figure 4A and an unpaired graph for CD69 (number of samples ranges from 9 to 32 depending on T_{reg} subset indicated) for HNSCC peripheral blood T_{regs} are shown. Paired non-parametric t-test (Wilcoxon) and non-parametric Kruskal-Wallis test were used, respectively. *p<0.05; **p<0.01; ****p<0.0001. **(C)** Representative staining of PBL T_{regs} for the markers in Fig. 4A and fig. S11A and B are shown. **(D)** The cutoff for high NRP1 expression in HNSCC PBL was defined by the distribution in HD PBL. The lines indicate the thresholds which is the mean (μ_{HD}) plus one or three standard deviations (σ_{HD}) from the healthy donor distribution for $NRP1^{SURF}$ and $NRP1^{TOT}$ (left and right, respectively). Table shown the differences in terms of number of samples above the threshold depending on cut point. The more stringent cut-off at $\mu_{HD}+3\ \sigma_{HD}$ was used for analyses. **(E)** $NRP1^{SURF}$ expression on PBL T_{regs} between patients that never progressed (n=69), progressed but are alive (n=6), or those who died due to their disease (n=10). Bar indicates the mean. Kaplan-Meier curve for $NRP1^{SURF}$ in PBL alone was evaluated as a predictor of disease specific survival (DSS). These data are associated with Fig. 4B. Curve comparison was executed using the logrank Mantel-Cox test. P-value with the hazard ratio (HR) ± the 95% confidence interval is reported. **(F)** A DSS Kaplan-Meier curve is shown for the cohort with matched PBL and TIL samples, corresponding to the cohort presented in Fig. 4E. Curve comparison was executed using the logrank Mantel-Cox test. P-value with the hazard ratio (HR) ± the 95% confidence interval is reported. **(G)** A Kaplan-Meier curve for progression-free survival is shown for the three groups defined in (C): low in both TIL and PBL (orange), high in only the TIL (black), and high in both TIL and PBL (blue). Disease-specific survival at 3 years is shown on right. Curve comparison was

conducted using a logrank Mantel-Cox test with the p-value corresponding to the comparison between all three curves shown in the interior of the graph. A forest plot showing the individual contributions of each factor to the overall Mantel-Cox result is shown. **(H)** A Kaplan-Meier curve for DSS is shown for the three groups defined in (C): low in both TIL and PBL (orange), high in only the TIL (black), and high in both TIL and PBL (blue). Disease-specific survival at 3 years is shown on right. Curve comparison was conducted using a logrank Mantel-Cox test with the p-value corresponding to the comparison between all three curves shown in the interior of the graph. A forest plot showing the individual contributions of each factor to the overall Mantel-Cox result is shown. **(I)** Similar to Fig. 4C but for values of $NRP1^{TOT}$ in PBL and TIL. **(J)** $NRP1^{TOT}$ expression on PBL T_{regs} between patients that never progressed (n=69), progressed but are alive (n=6), or those who died due to their disease (n=10). Bar indicates the mean. Progression-free survival and DSS curve comparisons were executed using the logrank Mantel-Cox test. P-value with the hazard ratio (HR) with a 95% confidence interval is reported.

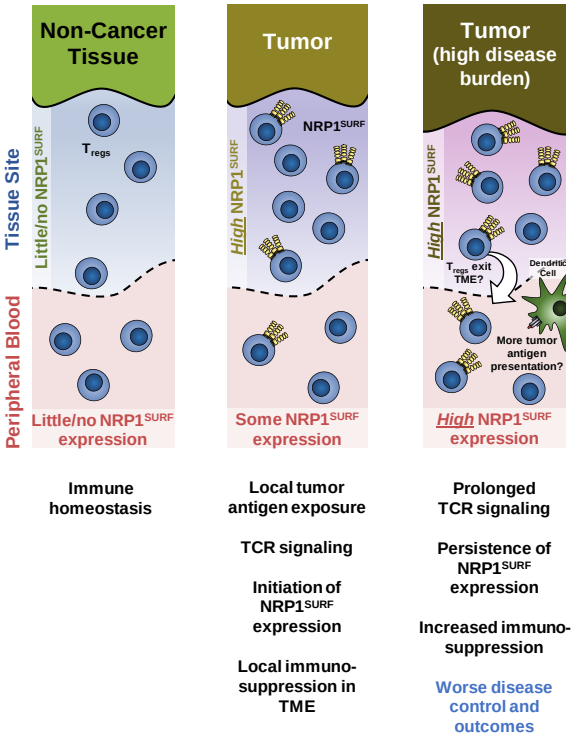

Fig. S13. T_{reg} NRP1 may reflect immune perturbation in cancer patients and potentiate disease by stabilizing T_{reg} function. Schematic summarizing our findings. T_{regs} in non-cancer tissue and the peripheral blood of healthy individuals express little to no NRP1; however, we observed marked $NRP1^{SURF}$ expression in patient tumors as well as in the peripheral blood. This expression is driven by TCR stimulation and supports potent immunosuppression. High prevalence of $NRP1^{SURF+}$ T_{regs} in peripheral blood is associated with high intratumoral $NRP1^{SURF+}$ prevalence and potentially increased disease burden, as this group of patients have worse PFS than those with increased $NRP1^{SURF+}$ T_{regs} in the tumor alone. Peripheral enrichment of $NRP1^{SURF+}$ T_{regs} may be mediated by higher rates of tumor antigen presentation in peripheral sites and thereby enhanced $NRP1^{SURF}$ persistence following tumor egress.

Table S1. Cancer patient clinical characteristics. Detailed information on patients with cancer in this study across all malignancies. Relevant clinical characteristics and lifestyle habits are recorded for each indication. N/A denotes not applicable for corresponding indication. For CRC mutation status, the total tally exceeds the patient total because most patients with BRAF or KRAS mutations were also confirmed to be microsatellite stable (MSS). HPV, human papillomavirus; MSS, microsatellite stable; EGFR, epidermal growth factor receptor; ALK, anaplastic lymphoma kinase; KRAS, Kirsten rat sarcoma virus; BRCA2, breast cancer 2; WT, wild-type. N/A denotes not applicable for corresponding indication.

		HNSCC		OvCa		NSCLC		CRC		PDAC		Melanoma	
Total patients		97		56		46		24		15		44	
Race	Caucasian	91		52		38		22		13		0	
	African American	4		3		1		1		1		0	
	Asian	0		0		1		1		0		0	
	Not reported/Other	2		1		6		0		1		44	
Histology / Site		Oral cavity	47	High grade serous	30	Adenocarcinoma	26	Adenocarcinoma	17	N/A		Malignant melanoma	18
				Low grade serous	3							Superficial spreading	10
		Oropharynx	27	Carcinosarcoma	7	Squamous	13	Mucinous adeno.	6			Nodular	7
				Endometrioid	6							Acral lentiginous	2
		Larynx	18	Clear cell	3	Neuroendocrine	1	Neuroendocrine	1			Epithelioid & spindle cell	1
		Hypopharynx	3	Mucinous carcinoma	3							In situ (& Hutchinson's Melanotic freckle)	3
		Other	2	Mixed / Other	4	Unknown	6	Unknown	0			Unknown	3
Stage	0 or 1	26		15		16		1		1		5	
	2	13		6		8		2		4		7	
	3	19		27		8		8		9		13	
	4	31		6		12		13		0		5	
	Not reported	8		2		2		0		1		14	
Tobacco Use	Never	19		N/A		5		15		7		N/A	
	Former	29				24		9		0			
	Current	49				17		0		8			
	Not reported	0				0		0		0			
Alcohol Use	Never	29		N/A		N/A		N/A		10		N/A	
	Former Heavy	8								0			
	Occasional	31								0			
	Current Heavy	29								3			
	Not reported	0								0			
Mutation Status		N/A		N/A		EGFR	2	MSS	21	KRAS	2	BRAF V600E	13
						ALK	0	BRAF+	1	KRAS, TP53	2	NRAS 61	2
						KRAS	1	BRAF-, Kras12/13+	4	BRCA2	1	Wild type	8
						None / Not determined	43	Not determined	1	WT or not determined	10	Not determined	21
HPV status	Positive	24		N/A		N/A		N/A		N/A		N/A	
	Negative	17											
	Not tested	56											

Table S2. Healthy donor clinical characteristics. All available information for healthy donor specimens utilized in this study. N/A denotes not applicable for corresponding indication. COPD, chronic obstructive pulmonary disease.

		Healthy Donor blood	Tonsil	Lung (normal)	Lung (COPD)	Ovary	Blood (ovarian cyst patients)
Total patients		30	9	9	6	14	17
Race	Caucasian	18	6	9	6	12	17
	African American	0	3	0	0	1	0
	Asian	0	0	0	0	0	0
	Not reported	12	0	0	0	1	0
Tobacco Use	Never	Not reported	4	8	0	N/A	N/A
	Former		0	0	0		
	Current		5	2	6		
	Not reported		0	0	0		
Alcohol Use	Never	Not reported	2	9	6	N/A	N/A
	Former Heavy		3	0	0		
	Occasional		1	0	0		
	Current Heavy		3	1	0		
	Not reported		0	0	0		